MINISTRY OF EDUCATION AND TRAINING

VIETNAM ACADEMY OF SCIENCE AND TECHNOLOGY

GRADUATE UNIVERSITY OF SCIENCE AND TECHNOLOGY

Dao Thi Bich Thao

DAMAGE DETECTION OF BEAM STRUCTURES USING CONCENTRATED OR MOVING MASSES BASED ON VIBRATION METHODS

SUMMARY OF DISSERTATION ON MECHANICAL ENGINEERING AND ENGINEERING MECHANICS

Major: Engineering Mechanics

Code: 9 52 01 01

Hanoi - 2026

The dissertation is completed at: Graduate University of Science and Technology, Vietnam Academy Science and Technology

Supervisor: Prof. Nguyen Viet Khoa

Referee 1:...

Referee 2:...

Referee 3:...

The dissertation is examined by Examination Board of Graduate University of Science and Technology, Vietnam Academy of Science and Technology at……………………….. (time, date……)

The dissertation can be found at:

1. Graduate University of Science and Technology Library
2. National Library of Vietnam

INTRODUCTION

1. Rationale for the research topic

During their service life, engineering structures are continuously subjected to severe external loads or repeated cyclic loading, which may induce localized damage or fatigue damage. Over time, such damage, particularly in the form of cracks, gradually propagates, leading to reductions in structural stiffness and load-carrying capacity. Once the damage reaches a critical level, failure to detect and repair it in a timely manner may result in structural collapse even under normal service conditions, causing catastrophic loss of life and substantial economic losses. Since structural damage alters the dynamic characteristics of a structure, such as its natural frequencies and mode shapes, vibration-based damage detection has received considerable research attention over the past decades, leading to the development and application of numerous damage identification techniques.

In recent years, vibration-based damage detection methods have received increasing attention for monitoring civil engineering structures owing to their significant advantages, including simple implementation, low cost, and non-destructive operation. Consequently, further development of vibration-based approaches toward practical applications in bridge and beam structures is both necessary and promising. Motivated by these considerations, this dissertation focuses on the topic: "Damage Detection of Beam Structures Using Concentrated or Moving Masses Based on Vibration Methods."

2. Research objectives

The objective of this dissertation is to develop vibration-based methods for damage detection to support the monitoring and early warning of structural safety hazards. The specific objectives are as follows:

- To develop a vibration-based method for detecting damage in Axially Functionally Graded (AFG) beams with varying cross-section, based on the variation of the beam's frequency response function under a concentrated mass.
- To develop a vibration-based damage detection approach for beam structures through the analysis of the vibration signal of a beam–moving mass system.

3. Research Contents

This dissertation investigates vibration-based damage detection methods for beam structures subjected to concentrated and moving masses. Chapter 1 reviews existing vibration-based damage detection methods and identifies the research gaps addressed in this dissertation. Chapter 2 develops the dynamic model of cracked AFG beams with variable cross-sections carrying concentrated masses and proposes a receptance-based method for crack localization using the Adomian Decomposition Method (ADM). Chapter 3 establishes the dynamic model of damaged beam–moving mass systems and proposes a wavelet transform-based method to identify the location, width, and severity of structural damage. Chapter 4 presents two experimental studies, and the agreement between numerical and experimental results verifies the accuracy and effectiveness of the proposed methods.

4. Original Contribution of the Dissertation

The dissertation has established the governing dynamic equations and derived an exact analytical expression for the receptance function of axially functionally graded beams with variable cross-sections containing cracks and carrying concentrated masses. It has also developed the governing dynamic equations for damaged beam–moving mass systems and solved them to obtain the dynamic responses of the coupled systems.

Based on the developed formulations, numerical simulations were conducted to investigate the combined effects of concentrated and moving masses on the dynamic characteristics of beam structures. The obtained results were then employed to propose a receptance-based method for crack detection in beams carrying concentrated masses and a wavelet transform-based method for damage detection in beams traversed by a climbing robot.

Chapter 1. LITERATURE REVIEW

This chapter reviews the current state of research on vibration-based structural damage detection. Since structural damage alters the dynamic characteristics of a structure, various vibration-based damage detection methods have been developed based on these changes. In practice, structural vibrations are often influenced not only by damage but also by additional factors such as concentrated or moving masses. Therefore, this chapter reviews and analyzes previous studies on the combined effects of structural damage and concentrated or moving masses on the dynamic characteristics of beam structures. Based on a critical assessment of the existing literature, the limitations and unresolved issues are identified, thereby establishing the research direction of this dissertation, namely the development of vibration-based damage detection methods for beam structures using concentrated or moving masses.

Chapter 2. DAMAGE DETECTION IN AFG BEAMS WITH VARYING CROSS-SECTION, CONTAINING A CRACK AND A CONCENTRATED MASS

This chapter investigates the effects of the AFG beam properties, cracks, and concentrated masses on the receptance function, and proposes a receptance-based method for crack detection in AFG beams.

2.1. Receptance function of a cracked AFG beam carrying a concentrated mass

Consider an Euler–Bernoulli beam with axially varying material properties carrying n concentrated masses m_i (i=1, … , n) as illustrated in Fig. 2.1. The beam is subjected to an external excitation force $f(t)$.

According to Wu *et al.* [60], the governing equation of transverse vibration can be expressed in the following non-dimensional $\xi = \dfrac{x}{L}$ form:

$$\left[E(\xi)I(\xi)y''\right]'' + L^4\rho(\xi)A(\xi)\ddot{y} + L^4\sum_{k=1}^{n} m_k\delta(\xi-\xi_{mk})\ddot{y} = L^4\delta\left(\xi-\xi_f\right)f(t) \tag{2.1}$$

where, E is the Young's modulus; I is the second moment of area, ρ is the mass density; $A(x)$ is the cross-sectional area; m_k is the k^{th} concentrated mass located at x_{mk}; $y(x, t)$ is the bending deflection of beam at location ξ and time t. $f(t)$ is the external excitation force acting at position x_f; $\delta\left(x-x_f\right)$ is the Dirac delta function.

Equation (2.1) may be regarded as the forced vibration equation of an unloaded beam subjected to the inertial forces generated by n concentrated masses with the external excitation $f(t)$. The solution of Eq. (2.1) can be found in the form:

$$y(\xi,t)=\sum_{i=1}^{\infty}\phi_i(\xi)q_i(t) \tag{2.2}$$

where, ϕ_i is i^{th} mode shape of the beam without concentrated masses and q_i is the i^{th} generalized coordinate.

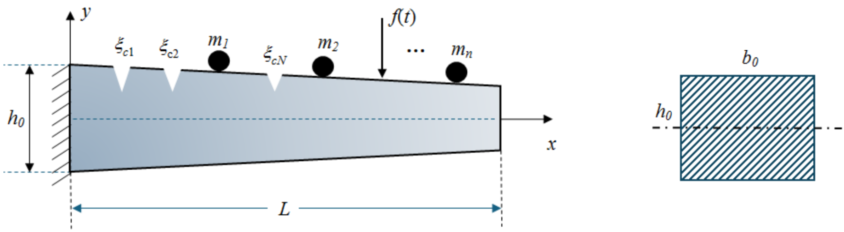

Fig. 2. 1. Euler–Bernoulli beam carrying n concentrated masses

Substituting Eq. (2.2) into Eq. (2.1), premultiplying both sides by $\phi_j(\xi)$ and integrating over the normalized beam length yield:

$$\mathbf{M}\ddot{\mathbf{q}}(t)+\mathbf{K}\mathbf{q}(t)=\mathbf{\Phi}(\xi_f)f(t) \tag{2.4}$$

where, **M** is the symmetric mass matrix and **K** is the diagonal stiffness matrix of order N. $\mathbf{\Phi}$, $\mathbf{q}$ the mode-shape vector and the generalized-coordinate vector of size $N\times 1$, respectively.

In the absence of external excitation, Eq. (2.4) reduces to:

$$\mathbf{M}\ddot{\mathbf{q}}(t)+\mathbf{K}\mathbf{q}(t)=\mathbf{0} \tag{2.5}$$

which represents the free-vibration equation of the beam carrying concentrated masses. The natural frequencies Ω are obtained by solving the corresponding eigenvalue problem.

When the beam is excited by a harmonic force $f(t)=\bar{f}e^{i\omega t}$, the receptance function measured at location ξ due to an excitation applied at ξ_f is given by:

$$\boldsymbol{\alpha}(\xi,\xi_f,\omega)=\frac{\mathbf{\Phi}^T(\xi)\bar{\mathbf{q}}}{\bar{f}}=\mathbf{\Phi}^T(\xi)\left(\mathbf{K}-\omega^2\mathbf{M}\right)^{-1}\mathbf{\Phi}(\xi_f) \tag{2.6}$$

where, $\mathbf{\Phi}^T(\xi)\overline{\mathbf{q}}$ and $\overline{f}$ denote the response amplitude at the measurement point ξ and the excitation force amplitude at the excitation point ξ_f, respectively.

It follows that once the mode shapes of the beam have been determined, the receptance function can be readily evaluated.

2.2. Mode shapes of the AFG beam with varying cross-section, containing a crack and a concentrated mass

Consider an Euler–Bernoulli AFG beam with a rectangular cross-section varying continuously along its longitudinal direction. The beam contains one or more transverse cracks and carries concentrated masses, as illustrated in Fig. 2.2.

The geometric dimensions and material properties vary along the beam according to:

$$\begin{aligned} E(\xi) &= E_0\left(1-\alpha_1\xi^{n_1}\right); \quad & b &= b_0\left(1-\alpha_2\xi^{n_2}\right) \\ h &= h_0\left(1-\alpha_3\xi^{n_3}\right); \quad & \rho &= \rho_0\left(1-\alpha_4\xi^{n_4}\right) \end{aligned} \tag{2.7}$$

where, E_0, b_0, h_0 and ρ_0 denote the Young's modulus, width, thickness, and mass density at the clamped end $\xi = 0$; $0 \le \alpha_i \le 1$, respectively; $n_i, i = \overline{1,4}$ are variation ratios of material properties of beam.

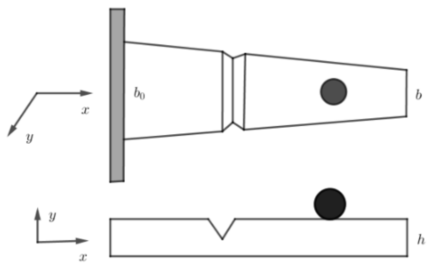

Fig. 2.2

When a crack is located at position $\xi_{cj}\left(0<\xi_{cj}<1\right)$ the bending stiffness *EI* is expressed as [7]:

$$E(\xi)I(\xi) = E(\xi)I(\xi)\left[1-f^*(\xi)\right] \tag{2.8}$$

inwhich,

$$f^*(\xi) = \sum_{j=1}^{N} \gamma_j \delta\left(\xi - \xi_{cj}\right) \tag{2.9}$$

and γ_j is the intensity of the j^{th} concentrated crack located at ξ_{cj}.

The mode shapes ϕ_i are obtained by solving the following eigenvalue problem:

$$\left\{E(\xi)I(\xi)\left[1-f^*(\xi)\right]\phi_i''(\xi)\right\}'' q_i(t) + L^4\mu(\xi)\phi_i(\xi)\ddot{q}_i(t) = 0 \tag{2.10}$$

The solution of the mode shape ϕ_i can be represented as an infinite convergent power series:

$$\phi_i(\xi) = \sum_{k=0}^{\infty} C_k \xi^k \tag{2.11}$$

with the corresponding terms being the coefficients to be determined C_k.

To derive the analytical solution, the linear differential operator $\ell = \dfrac{d^4}{d\xi^4}$ and the fourth-order integral operator $\ell^{-1} = \int_0^{\xi}\int_0^{\xi}\int_0^{\xi}\int_0^{\xi}(\ldots)d\xi d\xi d\xi d\xi$ are introduced. Consequently, the mode shape can be written as

$$\phi_i = \sum_{k=0}^{3} C_{0k}\xi^k + \ell^{-1}\{\mathcal{A}\} + \ell^{-1}\{\mathcal{B}\} \tag{2.12}$$

In this formulation, the first component $\mathcal{A}$ corresponds to the intact beam, whereas the second component $\mathcal{B}$ explicitly represents the influence of cracks. It is noteworthy that the crack-related terms only modify the first four coefficients of the power-series solution without affecting the remaining higher-order terms.

For an intact beam, the mode shape is simplified to:

$$\phi_i = \sum_{k=0}^{3} C_{0k}\xi^k + \ell^{-1}\{A\} \tag{2.13}$$

For a cracked beam, the crack-induced correction is superimposed onto the intact solution. Accordingly, the intact contribution and the crack contribution are derived independently and subsequently combined to obtain the complete analytical expression for the mode shape of the cracked beam.

The resulting mode shape is therefore expressed as

$$\phi_i = \sum_{k=0}^{3} C_{0k}\xi^k + \sum_{k=0}^{3}\left(\hat{b}_k + B_k^*\right)\xi^k + \sum_{k=4}^{\infty} C_k\xi^k = \sum_{k=0}^{3} C_k\xi^k + \sum_{k=4}^{\infty} C_k\xi^k \tag{2.14}$$

with,

$$C_k = C_{0k} + \hat{b}_k + B_k^* = b_k^* + B_k^*,\ k < 4 \tag{2.15}$$

The coefficients C_k ($k < 4$), which include the crack-dependent terms, b_k^*, B_k^* are determined from the boundary conditions together with the compatibility conditions imposed at the crack locations, respectively. The remaining coefficients C_k ($k \geq 4$) are obtained recursively from the solution corresponding to the intact beam.

2.3. Numerical simulation

2.3.1. Verification of the theoretical formulation

Table 2. 1. The normalized natural frequencies of intact AFG cantilever beams with variable thickness.

α_2		Ref. [127]			Present results			Eror(%)		
		Ω_1	Ω_2	Ω_3	Ω_1	Ω_2	Ω_3	Ω_1	Ω_2	Ω_3
0.8	n_2=1	-	-	-	6.211	22.835	53.562	-	-	-
	n_2=2	7.067	29.091	67.867	7.067	29.091	67.870	0.0	0.0	0.0044

In order to verify the accuracy of the theoretical formulation developed in this dissertation, a cantilever (C–F) beam composed of steel and aluminum, as reported in Ref. [127] is adopted. The material properties and beam thickness vary along the beam according to the following expressions:

$$E(\xi) = E_0\left(1-\alpha_1\xi^{n_1}\right),\ h = h_0\left(1-\alpha_2\xi^{n_2}\right),\ \rho(\xi) = \rho_0\left(1-\alpha_3\xi^{n_3}\right) \tag{2.16}$$

where, $n_1 = n_3 = 2$, $\alpha_1 = 1 - \frac{E_1}{E_0}$, $\alpha_3 = 1 - \frac{\rho_1}{\rho_0}$, α_2 varies from 0.2 to 0.8. The subscripts "$_0$" and "$_1$" denote the material and geometric properties at the left and right ends of the beam, respectively.

Table 2.1 shows that the present results are in excellent agreement with those reported in Ref. [127].

Fig. 2.3. Ratio of the second natural frequency

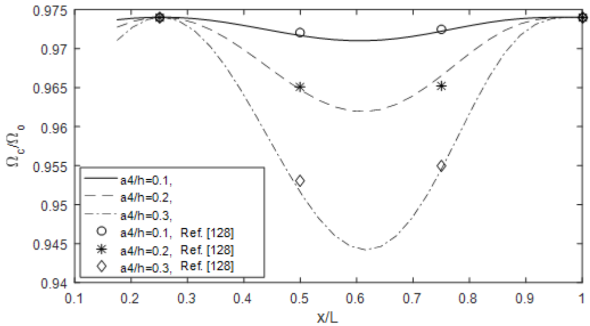

For the cracked beam, the natural frequencies are computed for a beam with four cracks located at $0.05L$, $0.1L$, $0.15L$, with the fourth crack position varying from $0.175L$ to $0.975L$, and with different crack depths: $a_1 = 0.3h$, $a_2 = 0.2h$, $a_3 = 0.1h$, a_4 varying from $0.1h$ to $0.3h$. The results are compared with Ref. [128]. The thickness variation coefficient is fixed at $\alpha_2 = 0.5$.

As illustrated in Fig. 2.3, the predicted natural frequency ratios agree remarkably well with those reported in Ref. [128], further demonstrating the validity of the proposed analytical formulation for cracked AFG beams.

2.3.2. Influence of the crack and material-property variation on the natural frequencies and mode shapes

a) *Influence of the crack and thickness variation on the natural frequencies*

A cantilever (C–F) axially functionally graded (AFG) beam with variable thickness containing four cracks located at positions $\xi_{c_1} = 0.34L$, $\xi_{c_2} = 0.5L$, $\xi_{c_3} = 0.7L$ and $\xi_{c_4} = 0.8L$ is considered. The crack depths vary from $0.0h$ to $0.4h$. The natural frequencies of the beam are calculated using the following material gradation parameter: $\alpha_1 = 0.5$, $\alpha_2 = 0.0 \div 0.8$, $\alpha_3 = 0.5$.

The results indicate that, for each thickness variation parameter, the natural frequencies decrease with increasing crack depth. As the thickness variation parameter increases, the first natural frequency increases, whereas the second and third natural frequencies decrease for the same crack depth. However, the combined effects of crack depth and the thickness variation parameter on the natural frequencies are nonlinear.

b) Influence of the crack and material properties on the natural frequencies of the beam

Both cantilever (C–F) and simply supported (H–H) AFG beams containing four cracks are investigated. The beam has four cracks at ξc_1=0.05L, ξc_2=0.1L, ξc_3=0.15L, ξc_4 varies from 0.175L to 0.975L, the depths of these cracks are: $a_1 = 0.3h$, $a_2 = 0.2h$, $a_3 = 0.1h$, $a_4 = 0.3h$. The beam thickness and width decrease progressively from the left end to the right end, with a thickness-variation coefficient $\alpha_2 = 0.5$.

The computed results show that, for both the C-F and H-H boundary conditions, the curves of the natural-frequency ratio tend to shift toward the end of the beam where Young's modulus is smaller and the mass density is larger. These results indicate that the natural frequency becomes more sensitive to cracks located on the side with larger mass density and smaller elastic modulus.

c) Influence of the crack and the cross-section variation coefficient on the mode shape

It is known that a crack causes a local distortion in mode shapes of beam, however, this distortion is small when crack size is small. In order to reveal the influence of cracks and taper parameter on mode shape, the wavelet transform which is very useful tool to analyze small distortions contained in signals will be applied.

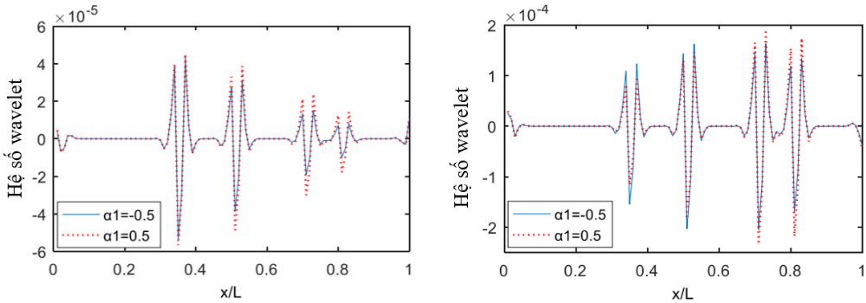

a) Crack depth = 0.3h, C-F   b) Crack depth = 0.3h, H-H

Fig. 2. 4. Wavelet transform of the first fundamental mode of beam with different boundary conditions

The results show that distinct peaks appear at the crack locations, indicating the influence of the crack on the mode shape. When the crack depths increase, the heights of these peaks also increase. For the C-F beam, the mode shape becomes more sensitive to cracks close to the free end, where the elastic modulus is smaller. For the H-H boundary condition, cracks located at smaller cross-sections have a greater influence on the mode shape of the beam.

2.3.3. Influence of the concentrated mass and the crack on the receptance function of the AFG beam

a) Influence of the crack on the receptance curvature

In this section, the effect of cracks on the receptance function is investigated through the receptance curvature, defined as the second derivative of the receptance function.

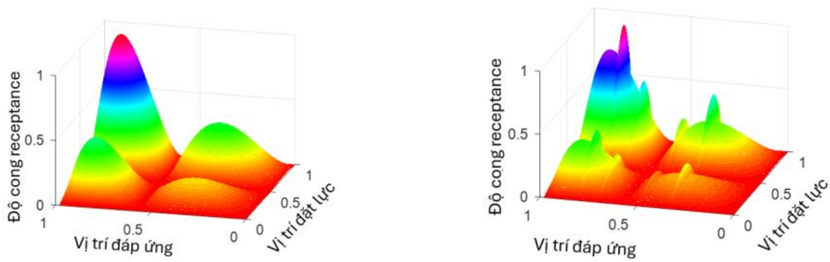

a) *Intact beam*, $\omega=\omega_2$ b) *Beam with a* 30% *crack*, $\omega=\omega_2$

Figure 2.5. Receptance curvature matrix of the H-H beam

Numerical results for the intact and cracked H–H beam with a crack depth of 30% show that the receptance curvature matrix of the intact beam varies smoothly, whereas that of the cracked beam exhibits distinct sharp peaks at the crack locations. These findings indicate that cracks induce localized disturbances in the receptance curvature matrix.

b) Simultaneous influence of the concentrated mass and the crack on the receptance curvature of the beam

The receptance curvature profile exhibits sharp peaks at the crack locations. However, for cracks of identical depth, the peaks located near the local minima of the receptance curvature are significantly smaller than those near the local maxima. A crack coinciding with a local minimum generates only a negligible peak, making its detection challenging. Moreover, peaks occurring in regions with lower receptance curvature maxima have smaller amplitudes than those in regions with higher maxima.

An attached concentrated mass can shift the local minima and maxima of the receptance curvature, thereby altering the relative positions between the crack-induced peaks and these extrema. Consequently, the amplitudes of the crack-induced peaks vary, with the extent of the variation depending on the location of the attached mass. Therefore, to enhance the detectability of cracks located near or coinciding with local minima, the concentrated mass should be placed at an appropriate location to shift the local minima away from the crack positions, move the local maxima closer to the cracks, or increase the amplitudes of the regions containing these cracks.

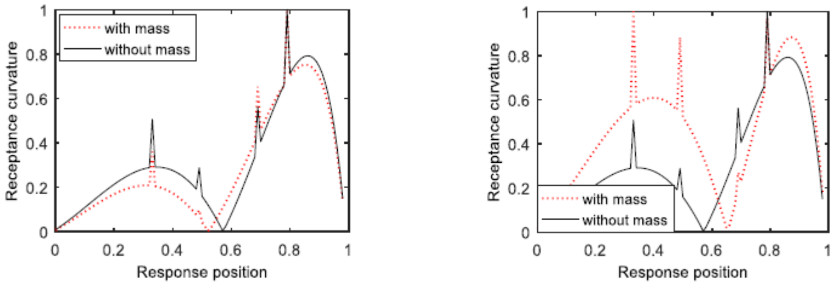

a) Mass location: $0.2L$ b) Mass location: $0.8L$

Fig. 2. 6. Receptance cuvature of H-H AFG beam, $\omega = \omega_2$.

2.4. Proposed method for crack detection in H-H AFG beams

Step 1: Measure the receptance-curvature function along the beam under harmonic excitation applied at a fixed location..

Step 2: Selected locations of the attached concentrated mass corresponding to the three excitation frequencies.

Step 3: Identify the sharp peaks appearing in the receptance-curvature curves. These localized peaks indicate the locations of structural cracks.

It should be noted that the location of the attached concentrated mass required to enhance weak crack-induced peaks or uncover peaks hidden at the nodal points of the receptance curvature is dependent on the beam boundary conditions.

2.5. Conclusions

In this chapter, the governing equations of motion were established for an axially functionally graded (AFG) beam with variable cross-section and material properties, containing a crack and carrying an attached concentrated mass. An exact mode shape function was derived in the form of a power series using ADM.

The analysis of the receptance curvature revealed the presence of sharp peaks at the crack locations, with the peak amplitudes increasing as the crack depth increased. These findings provide the theoretical basis for a crack detection method for AFG beams with variable cross-sections and material properties. Furthermore, it was demonstrated that placing a concentrated mass at appropriate locations can enhance the crack-induced peaks, thereby providing the foundation for a receptance-based crack detection method using an attached concentrated mass. The results presented in this chapter have been published in Publications Nos. 1–3, 5–7, and 11–12 listed in the “List of Publications Related to the Dissertation.”

Chapter 3. DAMAGE DETECTION IN BEAMS WITH A MOVING MASS

3.1. Model of a beam subjected to a moving robot

In this study, the circular beam is modeled as an Euler–Bernoulli beam. The beam–moving robot system under consideration is illustrated in Fig. 3.1.

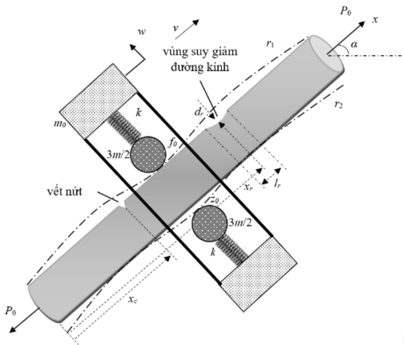

Fig. 3. 1. Model of a beam under the action of a moving robot.

inwhich,

z_0 is the vertical displacement of the beam at the contact point.

f_0 is the interaction force between robot and beam at the contact point.

u_{01} and u_{02} are displacements underneath the two wheels.

a) Equation of motion of the beam

The interaction between the beam and the moving robot constitutes a complex dynamic system. Therefore, the finite element method (FEM) is employed to determine the dynamic response of the beam–moving robot system. In the finite element model, the beam is discretized into equal-length elements of length $2l$. The effects of shear deformation and rotary inertia are neglected.

The governing equation of motion of the beam–robot system is expressed as follows:

$$\mathbf{m_e}\ddot{\mathbf{d}}_\mathbf{e} + \mathbf{k_e}\mathbf{d_e} + P_0\mathbf{k_{eg}}\mathbf{d_e} = \mathbf{f_e} \tag{3.1}$$

b) Equation of motion of the robot

In this work, we assume that the reduction in diameter of beam appears on only one surface at every position of the beam and the reduction in diameter can be expressed as the half sine wave function:

$$\begin{aligned} r_1(x) &= -d_{r1}rect(x)\sin\left[\frac{\pi(x - x_{r1})}{l_{r1}} + \frac{\pi}{2}\right] \\ r_2(x) &= -d_{r2}rect(x)\sin\left[\frac{\pi(x - x_{r2})}{l_{r2}} + \frac{\pi}{2}\right] \end{aligned} \tag{3.1}$$

he displacement beneath each wheel is given by:

$$u_{01} = z_0 + r_1 + \overline{r}_1;\ u_{02} = z_0 - r_2 - \overline{r}_2 \tag{3.3}$$

The equations of motion of the robot are derived by formulating its kinetic and potential energies and applying Lagrange's equations, as follows:

$$m_0\ddot{w} + k\left(2w - 2z_0 - r_1 - \overline{r}_1 + r_2 + \overline{r}_2\right) = 0 \tag{3.4}$$

c) *Equations of Motion of the Beam–Moving Robot System*

The displacement at the arbitrary position z_0 can be interpolate by applying the shape function as follows:

$$z_0 = \mathbf{N}\mathbf{d_e} \tag{3.5}$$

The motion equation of the beam-moving robot system can be written in the following form:

$$\mathbf{M}\ddot{\mathbf{D}} + \mathbf{KD} + \mathbf{K}_{eg}\mathbf{D} = \mathbf{f_e} \tag{3.6}$$

3.2. Cracked beam

When the beam contains a crack, the stiffness matrix of the beam–moving robot system is altered accordingly. For beams with circular cross-sections, the stiffness matrix of the cracked element is evaluated using the formulation developed by D. Y. Zheng [6].

The flexibility matrix of an intact beam element together with the additional flexibility introduced by a crack is written as:

$$\mathbf{c}^{(0)} = \begin{bmatrix} \dfrac{l^3}{3EI} & \dfrac{l^2}{2EI} \\ \dfrac{l^2}{2EI} & \dfrac{l}{EI} \end{bmatrix}; \mathbf{c}^{(1)} = \begin{bmatrix} \dfrac{F(1,1)}{2E'R} & \dfrac{F(1,2)L_c}{8E'R^3} \\ \dfrac{F(1,2)L_c}{8E'R^3} & \dfrac{F(2,2)}{8E'R^3} \end{bmatrix} \tag{3.7}$$

Accordingly, the flexibility matrix of the cracked beam element becomes:

$$\mathbf{c} = \mathbf{c}^{(0)} + \mathbf{c}^{(1)} \tag{3.8}$$

The corresponding stiffness matrix is then obtained as:

$$\mathbf{k_c} = \mathbf{T^T c^{-1} T} \tag{3.9}$$

For a beam with cracks, the global stiffness matrix **K** appearing in the governing equations of motion of the beam–moving robot system is assembled from the stiffness matrices of the cracked elements $\boldsymbol{k_c}$.

3.3. Numerical Simulations

This section presents numerical simulations of a beam with crack damage and cross-sectional diameter reduction subjected to a moving robot. The wavelet transform is applied to the dynamic displacement response of the beam–moving robot system to detect small damage in the beam.

3.3.1. Detection of Transverse Cracks

The beam properties adopted in the numerical simulations are: mass density ρ=7855 kg/m^3; Young's modulus E=2.1x10^{11} N/m^2; beam diameter d=0.2m; beam length: L=80m. The angle of inclination of the beam to the horizontal is 30^0. The depth and length of roughness can be calculated from Cheng *et al* (1999) as: $\bar{d}_{1,2} = -\dfrac{r_d(m_0 + 3m)gL^3}{48EI}$, $\bar{l}_{1,2} = \dfrac{L}{r_l}$ where, r_d=0.05 and r_l=5. The robot parameters are: m_0=15 kg; m=0.3 kg; k_1= k_2= k_3=1000 N/m; The displacement of the climbing robot is obtained to analyze the crack.

Figures 3.2-3.3 depict the dynamic displacements of the robot and their wavelet transforms with the tension force of the beam is P_0=5x10^6 N.

The numerical results indicate that, as the crack depth increases from 0% to 20%, the displacement response of the moving robot remains smooth, without noticeable local irregularities. Nevertheless, the wavelet transform of the robot displacement signal exhibits distinct peaks at the crack locations, and the amplitudes of these peaks increase as the crack depth increases.

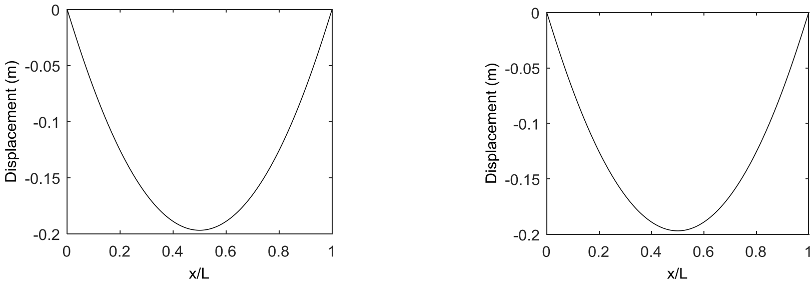

a) Crack depth = 0%　　　　b) Crack depth = 20%

Fig. 3.2. Displacement of robot for different crack depths

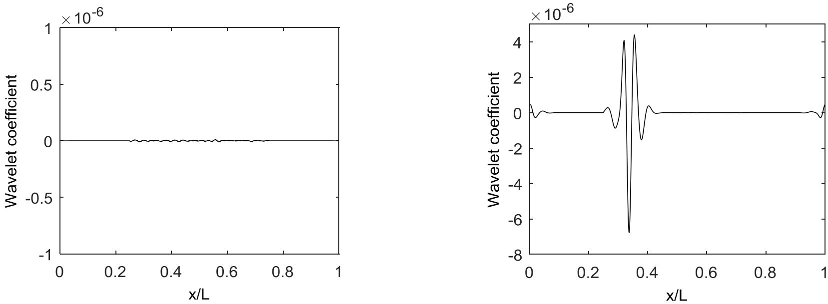

a) Crack depth = 0%　　　　b) Crack depth = 20%

Fig. 3.3. Wavelet transforms of the robot displacement for different crack depths

3.3.2. Detection of Local Diameter Reduction

It is assumed that there is one reduction in diameter on the upper surface with the center at $0.75L$, the length of reduction area is 0.1m, the amplitude of reduction area ranges from 0.1% to 5% of the beam diameter.

Figures 3.4 and 3.5 present the robot displacements and their wavelet transforms. As can be seen in this figures, when the amplitude of reduction is smaller than 0.5%, no distortion can be inspected visually from these displacements. However, the wavelet transforms of these displacements present clear peaks at the position of reduction area.

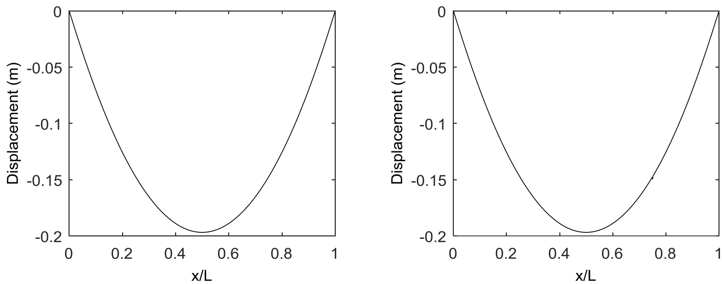

a) The amplitude of reduction: 0.1% b) The amplitude of reduction: 1%

Fig. 3.4. Displacement of robot for different amplitude of reduction

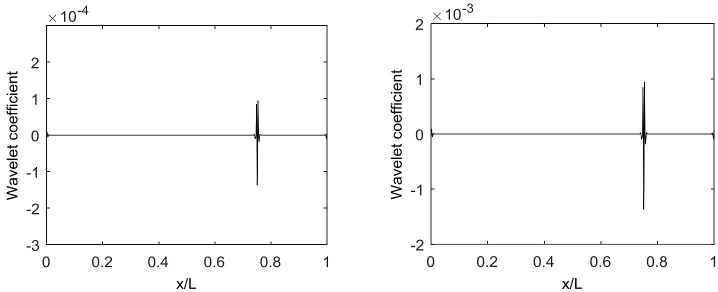

a) The amplitude of reduction: 0.1%. b) The amplitude of reduction: 1%

Fig. 3.5. Wavelet transforms of the robot displacement

3.3.3. Influence of the length of reduction area

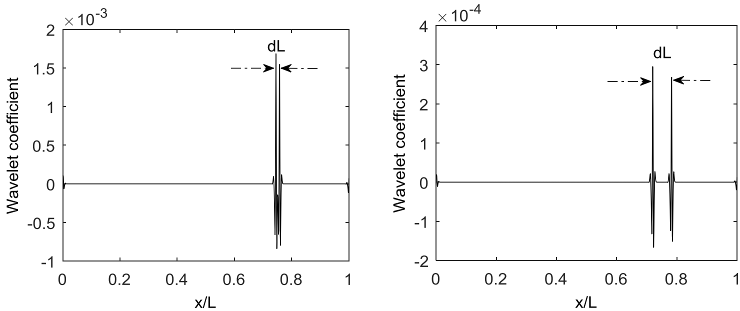

a) The length of reduction area: 1m b) The length of reduction area: 5m

Fig. 3.6. Wavelet transforms of the robot displacement for different the length of reduction area

Figure 3.6 illustrates the robot displacement response and the corresponding wavelet transform for a beam with a 5% cross-sectional diameter reduction, where the length of the damaged region ranges from 1m to 5m. The simulation results indicate that the local disturbance in the robot displacement response becomes less pronounced as the length of the damaged region increases. However, the damage can still be reliably identified by the distinct peaks appearing in the wavelet transform.

It is noted that the number of peaks and their heights in the wavelet transform depends on the length of reduction area. When the length of reduction area is small, for example l_r=0.1m, there is only one peak in the wavelet transform at the reduction area. However, when the length of the reduction area increases, these two sharp changes are separated leading to two separated peaks in the wavelet transform at the reduction area.

3.4. Proposed Damage Detection Procedure

Step 1: Mount a vibration sensor on the moving robot.

Step 2: Move the robot along the beam at a constant velocity, vvv.

Step 3: Measure the robot displacement response and transmit the acquired data to a computer.

Step 4: Perform wavelet analysis on the robot displacement data.

Step 5: Determine the location and the extent of the damaged region in the beam.

3.5. Conclusions

Chapter 3 established the governing equations of motion of the beam–moving robot system using the FEM to enable beam damage detection based on vibration signals acquired by sensors mounted on the moving robot. The effects of crack damage and cross-sectional diameter reduction on the vibration response of the moving robot were systematically investigated, providing the theoretical foundation for the development of beam damage detection methods. The results presented in this chapter have been published in paper 8 and 10 listed in the *List of Publications Related to the Dissertation*.

Chapter 4. EXPERIMENTAL VALIDATION

This chapter presents the experimental investigations conducted for two cases: an AFG beam carrying an attached concentrated mass and a cable–moving robot system.

4.1. Beam carrying an attached concentrated mass

4.1.1. Measurement of the Receptance Function of an AFG Steel Beam Carrying a Concentrated Mass

The parameters of the beam: Length: $L = 0.7$ m;

Constant thickness: $h = 0.01$ m.

Variable width: $b_0 = 0.03$m at the clamped end and $b_1 = 0.01$m at the free and.

A concentrated mass of: 0.6 kg.

To obtain a receptance curve at a given excitation frequency, the excitation force is applied at a fixed location on the beam, while the response is measured sequentially at 14 equally spaced measurement points by moving the sensor along the beam. The receptance curve is then constructed by plotting the receptance amplitude against the measurement location using the data acquired from the 14 measurement points.

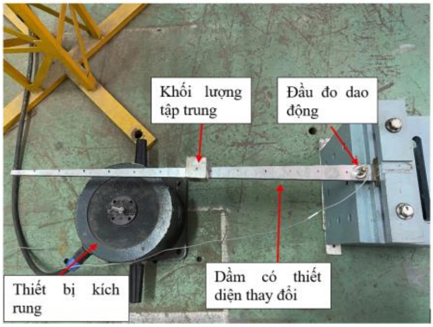

Fig. 4. 1. Experimental setup of the beam with an attached concentrated mass.

To determine the receptance matrix at a given excitation frequency, 14 receptance curves are measured by successively applying the excitation force at each of the 14 measurement locations on the beam.

4.1.2. Experimental Results

The receptance matrices of the variable cross-section beam, with and without an attached concentrated mass, obtained from the experiments are in good agreement with the numerical results.

The experimental results show that the receptance amplitude at the free end of the beam is significantly higher than that at the receptance peak. When an attached concentrated mass is introduced, the receptance matrix is altered compared with that of the beam without the concentrated mass. If the concentrated mass is placed at the receptance peak, the peak amplitude decreases significantly. In addition, the nodal points of the receptance are shifted toward the location of the attached concentrated mass.

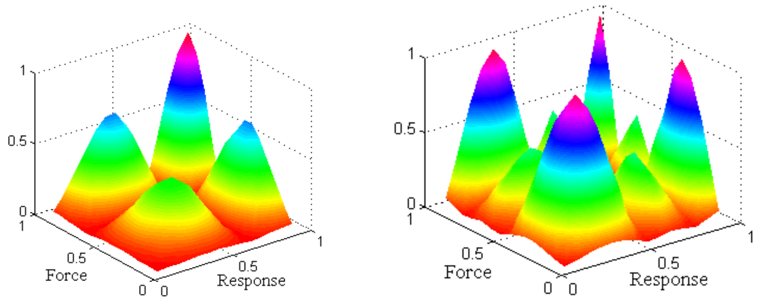

a) $\omega=\omega_2$, mass at position $L/2$; b) $\omega=\omega_3$, mass at position $2L/3$

Fig. 4. 2. Receptance matrices of the AFG cantilever beam with a mass

4.2. Experimental Validation for Cable Damage Detection Using a Moving Robot.

Testing on a real cable is beyond our lab's ability so we applied a plastic pipe for the test. The pipe has a length of 4m, a diameter of 0.1m and a thickness of 0.004mm. The traveling distance of robot is L=3m. The experimental setup is depicted in Fig. 4.3.

Three smooth reduction areas were made at 0.37L, 0.6L and 0.8L with different depths ranging from 1 mm to 2 mm, equivalent to 1% to 2% of the pipe's diameter. The first and second reduction areas were made on the upper side of the pipe while the third reduction area was made around the pipe. A robot weighing 7kg travels at a constant velocity of 0.38 m/s. Five experimental scenarios involving cable damage in the form of cross-sectional diameter reduction were conducted for validation.

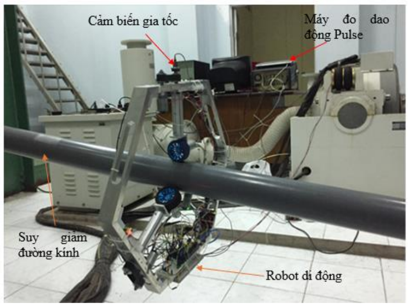

Fig. 4.3. Experimental setup

The experiments pointed out that, although the measured signals were polluted by the measurement noise, the vibration signal measured from the robot was very sensitive to the diameter reduction. Fig. 4.4 depicts the vibration measured from the robot and its wavelet transform in the first scenario in which the depth of the first and the second reduction areas are 1 mm and 2 mm, respectively. As can be seen from this figure, there are two significant peaks at the reduction areas but the vibration signal looks quite complicated. The peak at the first reduction area is not as clear as the peak at the second reduction area since the depth of the first reduction is smaller than that of the second reduction. However, the wavelet transform of this vibration signal shows two clear peaks at positions of $0.37L$ and $0.6L$ where the reductions areas located. The peak in the wavelet transform at the first reduction area is also smaller than the second peak.

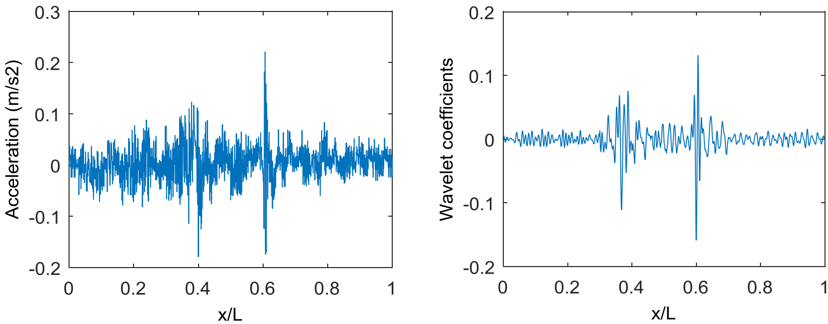

Fig. 4.4. Vibration signal of robot and its wavelet transform

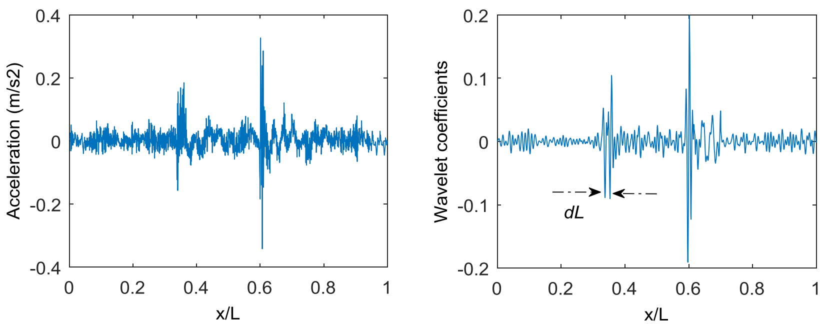

Fig. 4.5. Vibration signal of robot and its wavelet transform, the length of the first reduction area is 60mm.

As can be seen from Fig. 4.5, when the length of the first reduction area increases to 60mm, there are two separated peaks in the wavelet transform at the first reduction area as expected. Calculating from the graph of the wavelet transform, the length of gap between these two separated peaks is dL = 50 mm, i.e. 10mm smaller than the real reduction area. This can be explained by the fact that the diameter of pipe reduces smoothly from the starting and stopping points of the first reduction area and then becomes deepest at positions of about 5mm from the starting and stopping points. At these two positions there are significant changes in diameter leading to the significant influences on the vibration signal of robot. Thus, these significant changes will be detected and presented by significant peaks in the wavelet transform.

4.3. Conclusions

The experimental results demonstrate good agreement with the numerical predictions of the receptance function for beams with variable cross-sections. This agreement validates the accuracy and reliability of the exact formulation of the receptance function for axially varying beams carrying an attached concentrated mass developed in this dissertation.

The close agreement between the numerical and experimental results in the wavelet-based analysis of cable damage further confirms the validity of the governing equations of motion for the beam–moving mass system developed in this dissertation. Moreover, these findings demonstrate the potential of applying cable-climbing robots to vibration-based damage detection in stay cables of cable-stayed bridges.

The results presented in this chapter have been published in Paper 4 and 8–10 listed in the “List of Publications Related to the Dissertation”.

CONCLUSIONS

This dissertation has established the governing dynamic equations for AFG beams with variable cross-sections containing transverse cracks and carrying concentrated masses. By solving these equations, exact analytical expressions for the mode shapes and the receptance function were derived. The developed receptance formulation was subsequently employed in extensive numerical simulations to investigate the combined effects of structural cracks and concentrated masses on the dynamic characteristics of AFG beams.

In addition, a finite element formulation was developed for damaged beam structures subjected to moving masses. The governing equations of the coupled beam–moving robot system were established and solved numerically to obtain the dynamic responses of the system. Based on these responses, comprehensive numerical investigations were carried out to evaluate the influences of transverse cracks and localized cross-sectional reductions on the vibration behavior of the coupled system.

Based on the analytical and numerical investigations, two vibration-based damage detection methods have been proposed.

(i) A receptance-based crack detection method for beams carrying an attached concentrated mass is proposed. The concentrated masses are strategically placed to shift the peaks and nodal points of the receptance curvature. As a result, weak crack-induced peaks located near the nodal points are amplified, thereby facilitating crack detection. In addition, peaks that are concealed when the crack location coincides with a nodal point become distinguishable and are subsequently enhanced.

(ii) A wavelet-based method is proposed for detecting crack-type damage and cross-sectional diameter reduction in beam subjected to excitation from a moving robot. As the robot passes through damaged regions, the wavelet transform of the robot vibration signal exhibits distinct peaks at the corresponding damage locations. The damage locations are then determined based on the robot velocity. For diameter-reduction damage, the distance between the peaks corresponding to the beginning and the end of the damaged region is further used to estimate the extent of the diameter reduction.

Experimental investigations were conducted for two cases: an AFG beam with a variable cross-section carrying an attached concentrated mass and a damaged cable with cross-sectional diameter reduction subjected to a moving mass. The experimental results show good agreement with the numerical predictions, thereby validating the theoretical formulations of the exact mode shape function and the receptance function for AFG beams developed in this dissertation. Furthermore, the experimental results demonstrate the potential of cable-climbing robots for vibration-based damage detection in the stay cables of cable-stayed bridges.

Original Contributions

1. The governing equations of motion were established, and an exact formulation of the receptance function was derived for axially functionally graded (AFG) beams with variable cross-sections and material properties, containing cracks and carrying an attached concentrated mass.

2. The governing equations of motion were developed for a beam–moving mass system in which the beam contains damage in the form of cracks and cross-sectional diameter reduction. The dynamic responses of the system were subsequently obtained by solving the governing equations.

3. Based on the developed formulations, comprehensive numerical simulations were performed to investigate the combined effects of an

attached concentrated mass and a moving mass on the dynamic characteristics of the beam. On the basis of these results, a receptance-based crack detection method employing an attached concentrated mass and a wavelet-based damage detection method for beams carrying a mobile robot were proposed.

Future research directions

Although this dissertation has derived an exact formulation for the receptance function of cracked AFG beams with an attached concentrated mass, the formulation is currently limited to AFG beams whose axial material properties or cross-sectional variations are represented by polynomial functions. Future research should extend the proposed approach to other AFG beam configurations, such as AFG beams integrated with surface-bonded piezoelectric layers or beams with axial property variations following sinusoidal, exponential, or other functional distributions

In addition, this dissertation has considered only AFG beams carrying a fixed concentrated mass. The more general case involving multiple moving concentrated masses remains unresolved and deserves further investigation. Experimental validation of the proposed methods for AFG beams should also be conducted as advances in manufacturing technologies make the fabrication of AFG beams increasingly feasible.

Furthermore, the application of cable-climbing robots for vibration-based cable damage detection is still at an early stage. Existing studies primarily focus on individual damage types, such as cracks or diameter reduction, whereas the coupled effects of multiple damage mechanisms have yet to be fully understood and should be investigated in future research. Moreover, integrating wavelet-based analysis with advanced artificial intelligence (AI) techniques represents another promising direction for further development of the research presented in this dissertation.

LIST OF PUBLICATIONS RELATED TO THE DISSERTATION

The results of the dissertation have been published in international journals, national journals, and proceedings of specialized scientific conferences, both domestic and international, as follows:

1. Khoa Viet Nguyen, Thao Thi Bich Dao, 2026, Modified method for deriving the receptance function of a cracked nonuniform AFG beam carying concentrated masses and its application for crack detection, *European Journal of Mechanics – A/Solids*, 116, 105947. (SCIE, Q1)

2. Khoa Viet Nguyen, Thao Thi Bich Dao, Quang Van Nguyen, 2024, Exact solution for mode shapes of cracked nonuniform axially functionally graded beams, *Mechanics Research Communications*, 139, 104306. (SCIE, Q2)

3. Nguyễn Việt Khoa, Đào Thị Bích Thảo, Nguyễn Văn Quang, Vũ Đỗ Long, 2024, Công thức dạng riêng chính xác cho dầm AFG bị nứt có thiết diện thay đổi, *Hội nghị Khoa học kỷ niệm 50 năm thành lập Viện Hàn lâm KH&CN Việt Nam, Tiểu ban Công nghệ thông tin, Điện tử, Tự động hóa, Khoa học và Công nghệ vũ trụ*, Hà Nội, 14/3/2025.

4. Đào Thị Bích Thảo, Nguyễn Việt Khoa, Nguyễn Văn Quang, Vũ Đỗ Long, 2024, Nghiên cứu bằng thực nghiệm hàm phổ phản ứng của dầm có chiều cao thay đổi. *Hội nghị Cơ học Toàn quốc Kỷ niệm 45 năm thành lập Viện Cơ học, Hà Nội, 09/4/2024*, pp. 513- 523.

5. Nguyễn Việt Khoa, Đào Thị Bích Thảo, Nguyễn Văn Quang, 2024, Nghiên cứu, so sánh đặc trưng động lực học của dầm AFG có chiều cao với dầm có chiều rộng thay đổi. *Hội nghị Cơ học Toàn quốc Kỷ niệm 45 năm thành lập Viện Cơ học, Hà Nội, 09/4/2024*, pp. 407- 416.

6. Thao Thi Bich Dao, Khoa Viet Nguyen, Quang Van Nguyen, 2023, Exact receptance function of tapered AFG beam with nonlinearly varying ratio of beam properties carrying concentrated masses, *Vietnam Journal of Mechanics*, Vol.45, No.4, pp. 296-317.

7. Khoa Viet Nguyen and Thao Thi Bich Dao, 2023, Exact receptance function of a cracked axially functionally graded beam, *The 7th International Conference on Engineering Mechanics and Automation 2023*.

8. Thao Thi Bich Dao, Khoa Viet Nguyen, Quang Van Nguyen and Long Do Vu, 2023, Theoretical and experimental studies on the receptance function of a nonuniform AFG beam, *The 7th International Conference on Engineering Mechanics and Automation 2023*.

9. Khoa Viet Nguyen, Ngoc Van Bach Pham and Thao Thi Bich Dao, 2022, Damage detection of cables in cable-stayed bridge using vibration data measured from climbing robot, *Advances in Structural Engineering*, 2022, Vol 25(13), pp. 2705-2721. (SCIE, Q1)

10. Khoa Viet Nguyen, Thao Thi Bich Dao and Quang Nguyen Van, 2022, Influence of the varying axial force on the detection of diameter reduction of bridge cables using climbing robot, *Tuyển tập công trình Hội nghị Cơ học toàn quốc lần thứ* XI, Hà Nội, 02-03/12/2022.

11. Thao Thi Bich Dao, Khoa Viet Nguyen and Long Do Vu, 2022, Receptance function of an axially functional graded beam with varying width using Adomian method, *Tuyển tập công trình Hội nghị Cơ học toàn quốc lần thứ XI*, Hà Nội, 02-03/12/2022.

12. Khoa Viet Nguyen, Thao Thi Bich Dao, Long Do Vu and Quang Van Nguyen, 2021, Exact receptance and receptance curvature functions of the axially load cracked beam carrying concentrated mass, *The 6th International Conference on Engineering Mechanics and Automation* (ICEMA6), 2021.